A conservative model for high-throughput synthesis of nanoparticles in reacting gas flows

Jean-Maxime Orlac'H, Nasser Darabiha, Vincent Giovangigli, Benedetta Franzelli

▶ **To cite this version:**

Jean-Maxime Orlac'H, Nasser Darabiha, Vincent Giovangigli, Benedetta Franzelli. A conservative model for high-throughput synthesis of nanoparticles in reacting gas flows. 2019. hal-03006167v1

HAL Id: hal-03006167

https://hal.science/hal-03006167v1

Preprint submitted on 22 Nov 2019 (v1), last revised 15 Nov 2020 (v3)

HAL is a multi-disciplinary open access archive for the deposit and dissemination of scientific research documents, whether they are published or not. The documents may come from teaching and research institutions in France or abroad, or from public or private research centers.

L'archive ouverte pluridisciplinaire **HAL**, est destinée au dépôt et à la diffusion de documents scientifiques de niveau recherche, publiés ou non, émanant des établissements d'enseignement et de recherche français ou étrangers, des laboratoires publics ou privés.

A conservative model for high-throughput synthesis of nanoparticles in reacting gas flows

Jean-Maxime Orlac'h*,[1], Nasser Darabiha[1], Vincent Giovangigli[2], and Benedetta Franzelli[1]

[1]EM2C laboratory, CNRS, Ecole CentraleSupélec, 8-10 rue Joliot Curie, 91190 Gif-sur-Yvette, France
[2]CMAP, CNRS, Ecole Polytechnique, 91128 Palaiseau, France

November 5th 2019

Abstract

Considerable progress has been made over the past decades in the modeling of gas-phase synthesis of nanoparticles. However, when the nanoparticles mass fraction is large representing up to 50 % of the mixture mass fraction, some issues can be observed in the self-consistent modeling of the production process. In particular, enthalpy exchanges between gas and particle phases and differential diffusion between the two phases are usually neglected, since the particle mass fraction is generally very small. However, when high nanoparticle mass fractions are encountered, these simplifications may cause non conservation of the total enthalpy or the total mass. In the present paper, we propose a conservative model for nanoparticles production from gas-phase processes with a high throughput of nanoparticles. The model is derived in order to satisfy conservations of both enthalpy and mass and is validated on laminar one-dimensional premixed and non-premixed flames. In particular, it is shown that the enthalpy of the particle phase as well as the differential diffusion of the gas phase with respect to the particle phase cannot be generally neglected when the nanoparticles concentration is high to preserve the accuracy of the numerical results.

Introduction

Flame processes are widely used for the manufacture of several nano-structured commodities, such as titanium dioxide – titania –, carbon black and fumed silica [1,2], representing a billion dollar industry. Nanoparticle synthesis requires a fine control of the particle size and shape distribution, and of the nanoparticle crystal phase with desired properties depending on the applications targeted. Therefore, detailed modeling is of critical importance for the optimization of nanoparticle production in flame reactors.

The nanoparticle phase is generally described as an aerosol characterized by its size distribution, with approaches very similar to the ones used in the modeling of soot particles in flames, e.g. Monte Carlo methods, sectional or moment methods [3,4]. However, in sooting flames the particle mass fraction is very often negligible, whereas in industrial processes for nanoparticle synthesis the

*Corresponding author: jean-maxime.orlach@centralesupelec.fr

nanoparticle density can be comparable to that of the gas phase. Yet, models classically used for soot in flames generally do not satisfy the overall conservation of mass and energy in the mixture as a whole. This has no influence on the results, given the very low soot concentrations observed in practice. On the contrary, when dealing with highly concentrated aerosols – "highly concentrated" implies here that the nanoparticle mass or mole fraction is comparable to that of the gas phase – such as titania nanoparticles, it is required to satisfy the overall conservation of mass and energy in the multiphase flow.

In the present work, we study the modeling of titania nanoparticle production in laminar flames at high concentration. Titanium dioxide is used as a white pigment – e.g. in paintings, solar creams, cosmetics – as a catalyst support, and as a photocatalyst. Even if in most laboratory-scale experimental studies of titania nanoparticles flame synthesis, the precursor concentration generally represents a few percent of the oxidizer flow rate [5–7], industrial aerosol reactors are usually operated at high precursor mass fraction, possibly more than 50% of the oxidizer flow rate [8,9]. Since the reaction yield is rather high as up to 50% of the injected precursor can be converted into TiO_2 powder [7], the mass fraction of the particle phase can be non-negligible in comparison to that of the gas phase. This may yield a possible strong coupling between both phases, such that exchanges of mass and energy between the two phases will no longer be negligible. Other types of nanoparticles are also concerned with high conversion yield and high concentration, e.g. SiO_2 nanoparticles produced from $SiCl_4$ [10–12] or HMDSO [13]. Here, we focus on titania nanoparticles as a representative test case.

Concerning the synthesis of titania nanoparticles in reacting flows, a strong effort has been dedicated to the development of accurate and efficient numerical models over the past decades. As a first approach, only the particle phase can be accounted for while prescribing the experimental temperature profiles. In that case, no equations are solved for enthalpy, fluid flow velocity, or gaseous species mass fractions, and the state of the gas corresponding to experimental measurements is taken as an input to the nanoparticle model. Therefore, it is not necessary to model self-consistently the gas phase to ensure conservation of the mixture mass and enthalpy. For this, 0D reactors [9,14–17] or arrays of 0D reactors models are considered, assuming that the turbulent mixing is dominant compared to differential diffusion which can be neglected [18–21].

Some studies have accounted for a two-way coupling between the gas and particle phases by incorporating in the gas phase a pseudo gas component representing the overall nanoparticle mass fraction [22], thereby ensuring the global conservation of enthalpy and mass. A pseudo gas component is also routinely used in tabulation processes employed for Large-Eddy Simulation (LES) [20,23,24]. It is worth noting that when the flow is turbulent, thermophoresis can be neglected as particles transport is dominated by convection and turbulent transport [22–25]. However, conservation of mass is not always fulfilled in tabulated LES models, and in some cases it may even be necessary to adapt the model in order to avoid consuming more $TiCl_4$ than available [23,24].

Other authors have employed fully two-way coupled models, without any pseudo gas component [25–27]. Among them, Wang and Garrick neglected enthalpy exchanges between the gas and particle phases [26,27]. On the contrary, other authors [25,28] solved the equation for the enthalpy of the gas phase accounting for an energy exchange term between the gas and particle phases to ensure global energy conservation. Unfortunately, the expressions for such exchange terms are not well known and they generally rely on ad hoc assumptions introducing additional uncertainties. In general, without any of the previous simplifying assumptions, the conservation of mass and enthalpy are not guaranteed. Therefore, a more general formulation, fully conservative in both mass and energy, would be desirable.

In the present paper, we present a conservative model for highly concentrated aerosol reactors. We will show that the use of non-conservative models can yield numerical instabilities, in particular when using a fully implicit solver. Neglecting the contribution of the particle phase to the mixture enthalpy may lead to significant errors in numerical simulations of nanoparticle synthesis in flames.

For this, we consider one-dimensional laminar premixed and counterflow flames. Such idealized flame configurations are the simplest possible, so that the conservation of enthalpy or mass will be assessed more easily. Laminar flames are indeed simpler than turbulent flames, where the nanoparticle kinetics can be strongly affected [29,30]. Besides, many turbulent flame models rely on preliminary one-dimensional calculations on idealized cases, so that accurately modeling 1D premixed and counterflow flames is a necessary step before adressing the modeling of more complex turbulent flames.

The paper is organized as follows. In section 1, a detailed model is presented and shown to ensure the conservation of both mass and enthalpy. In section 2, we detail the test cases adopted here, namely titania nanoparticle production from $TiCl_4$ in one-dimensional (1D) laminar methane-oxygen flames. In section 3 the conservation of enthalpy is studied in premixed flames. Finally, in section 4, the effect of differential diffusion on 1D non-premixed flames is considered in addition to the enthalpy conservation.

1 Dispersed phase conservative model

In this section, we present a conservative model for nanoparticle transport at high concentration. This model is general and can be applied through any type of Eulerian description, e.g. sectional, moment or Monte Carlo methods. We present first in subsection 1.1 the most general continuous formulation of the dispersed phase conservative model, where the nanoparticles are described by the continuous General Dynamic Equation. Then, in subsection 1.2 the model is detailed for the sectional method.

When high volume fractions are encountered, the dynamics of nanoparticles can be different compared to dilute aerosols [9,31]. Even at high aerosol mass fractions, the nanoparticles volume fraction remains low in general because the density of each individual nanoparticle is much larger than the average gas density. However, high level of fractality can have a strong effect on the nanoparticles dynamics as it increases the effective volume fraction occupied by the aerosol. It can in particular significantly affect the collision frequencies, or even lead to gelation of the aerosol [9]. Here, for the sake of simplicity, we neglect the nanoparticles fractality, so that the effective particle volume fraction remains low, and the aerosol remains in the dilute regime. In that case, the aerosol General Dynamic Equation [32] remains valid. However, the conservative model presented here could be easily adapted to any kind of aerosol kinetic equation, provided that such an equation is known.

1.1 Continuous formulation

We consider here that the two phases are in thermal and mechanical equilibrium, so that the velocities of the gas – subscript g – and solid particle – subscript p – phases are equal:

$$\boldsymbol{u}_{\mathrm{g}} = \boldsymbol{u}_{\mathrm{p}} = \boldsymbol{u}, \tag{1.1}$$

where $\boldsymbol{u}$ is the mixture-averaged velocity, and their temperatures coincide:

$$T_{\mathrm{g}} = T_{\mathrm{p}} = T, \tag{1.2}$$

where T is the mixture temperature. These assumptions are generally made in the modeling of fine particle transport.

This allows to treat the mixture as a unique dispersed phase, whose components can be either gas-phase molecular species or solid-state nanoparticles. In this so-called "one-mixture" model, the classical equations for conservation of mass and enthalpy of a multicomponent gas mixture are

retained, but the mixture density and enthalpy must now include both the gas and particle phases contributions. Here, the nanoparticles are modeled by means of a – discrete – sectional model. The mixture density reads:

$$\rho = \rho_{\mathrm{g}} + \rho_{\mathrm{p}}. \tag{1.3}$$

where ρ_{g} and ρ_{p} are the mass densities of the gas and solid particle mixtures, respectively:

$$\rho_{\mathrm{g}} = \sum_{k=1}^{N_{\mathrm{g}}} \rho_k, \tag{1.4}$$

$$\rho_{\mathrm{p}} = \int \rho_{\mathrm{s}}\, q(v)\, \mathrm{d}v. \tag{1.5}$$

The internal variable v represents the nanoparticle volume, N_{g} denotes the number of gas-phase species, $q(v) = vn(v)$ (in $\mathrm{cm}^3.\mathrm{cm}^{-3}$) is the volume density of the aerosol where $n(v)$ is the number density, and ρ_{s} is the density of a solid particle. The k^{th} species mass fraction Y_k and the mass fraction $Y(v)\,\mathrm{d}v$ of nanoparticles whose volume lies in the range $[v, v + \mathrm{d}v]$ are respectively defined as:

$$Y_k = \frac{\rho_k}{\rho}, \quad k = 1, \ldots, N_{\mathrm{g}}, \tag{1.6}$$

$$Y(v)\,\mathrm{d}v = \frac{\rho_{\mathrm{s}}\, q(v)}{\rho}\,\mathrm{d}v. \tag{1.7}$$

The mass conservation of the mixture as a whole implies that the mass fractions sum to unity:

$$\sum_{k=1}^{N_{\mathrm{g}}} Y_k + \int Y(v)\,\mathrm{d}v = 1. \tag{1.8}$$

We also introduce the gas and particle mass fractions:

$$Y_g = \sum_{k=1}^{N_{\mathrm{g}}} Y_k, \tag{1.9}$$

$$Y_p = \int Y(v)\,\mathrm{d}v. \tag{1.10}$$

so that equation (1.8) can also be written

$$Y_{\mathrm{g}} + Y_{\mathrm{p}} = 1. \tag{1.11}$$

The particles volume fraction is given by:

$$f_{\mathrm{v}} = \int q(v)\,\mathrm{d}v = \frac{\rho Y_{\mathrm{p}}}{\rho_{\mathrm{s}}}. \tag{1.12}$$

The conservation equations of mass, species and particle mass fractions then read:

$$\frac{\partial \rho}{\partial t} + \boldsymbol{\nabla} \cdot (\rho \boldsymbol{u}) = 0, \tag{1.13}$$

$$\frac{\partial (\rho Y_k)}{\partial t} + \boldsymbol{\nabla} \cdot (\rho Y_k \boldsymbol{u} + \rho Y_k \boldsymbol{\mathcal{V}}_k) = W_k \dot{\omega}_k, \quad k = 1, \ldots, N_{\mathrm{g}}, \tag{1.14}$$

$$\frac{\partial (\rho Y(v))}{\partial t} + \boldsymbol{\nabla} \cdot (\rho Y(v) \boldsymbol{u} + \rho Y(v) \boldsymbol{\mathcal{V}}(v)) = \rho_{\mathrm{s}}\, \dot{q}(v), v \in]0, +\infty[, \tag{1.15}$$

where W_k (g.mol^{-1}) is the k^{th} species molar mass, $\dot{\omega}_k$ (mol.cm^{-3}.s^{-1}) is the k^{th} species molar production rate, and $\boldsymbol{\mathcal{V}}_k$ (cm.s^{-1}) is the k^{th} species diffusion velocity. $\boldsymbol{\mathcal{V}}(v)$ (cm.s^{-1}) is the diffusion velocity of particles whose volume lies in the range $[v, v+\mathrm{d}v]$, and $\dot{q}(v)$ (cm^{-3}.s^{-1}) is the volumetric particle source term. Equation (1.15) is simply the General Dynamic Equation for aerosols. The mass exchange between the phases imposes:

$$\sum_{k=1}^{N_{\text{g}}} W_k \dot{\omega}_k + \int \rho_{\text{s}}\, \dot{q}(v)\, \mathrm{d}v = 0. \tag{1.16}$$

Therefore, to ensure mass conservation, the diffusive fluxes must sum to zero:

$$\sum_{k=1}^{N_{\text{g}}} \rho Y_k \boldsymbol{\mathcal{V}}_k + \int \rho Y(v) \boldsymbol{\mathcal{V}}(v)\, \mathrm{d}v = 0, \tag{1.17}$$

so that the constraint (1.8) is satisfied [33]. The system is closed by the perfect gas law

$$\rho = \frac{p\overline{W}}{RT}, \tag{1.18}$$

where p is the pressure, R is the universal constant, and $\overline{W}$ is the mean molar mass of the mixture, given by

$$\frac{1}{\overline{W}} = \sum_{k=1}^{N_{\text{g}}} \frac{Y_k}{W_k} + \int \frac{Y(v)}{W(v)}\, \mathrm{d}v, \tag{1.19}$$

where $W(v) = \rho_{\text{s}}\, v\, \mathcal{N}_{\text{A}}$ is the molar mass of the particles whose volume lies in the range $[v, v+\mathrm{d}v]$, with $\mathcal{N}_{\text{A}}$ the Avogadro number.

In the present work, the diffusion velocities of the gas-phase species and nanoparticles are defined by:

$$\boldsymbol{\mathcal{V}}_k = -D_k\, \boldsymbol{\nabla} \ln X_k + \boldsymbol{u}_{\text{cor}}, \tag{1.20}$$

$$\boldsymbol{\mathcal{V}}(v) = \boldsymbol{v}_{\text{th}} - D(v) \boldsymbol{\nabla} \ln Y(v) + \boldsymbol{u}_{\text{cor}}, \tag{1.21}$$

where D_k is the k^{th} species diffusion coefficient, X_k is the k^{th} species mole fraction, $\boldsymbol{v}_{\text{th}}$ is the thermophoretic velocity [34], and $D(v)$ is the diffusion coefficient of particles whose volume lies in the range $[v, v+\mathrm{d}v]$. To ensure the overall mass conservation, a correction velocity $\boldsymbol{u}_{\text{cor}}$ is adjusted to satisfy the constraint (1.17). The particle thermophoresis velocity is taken from Waldmann [35] as $\boldsymbol{v}_{\text{th}} = -C_{\text{th}}\, \nu\, \boldsymbol{\nabla} \ln T$, where $C_{\text{th}} = 3/4(1+\pi\alpha_{\text{T}}/8)^{-1} \approx 0.554$, and ν is the gas kinematic viscosity.

The – isobaric – conservative balance equation for the mixture enthalpy can be written as:

$$\frac{\partial(\rho h)}{\partial t} + \boldsymbol{\nabla} \cdot (\rho h \boldsymbol{u}) + \boldsymbol{\nabla} \cdot \Big(-\lambda \boldsymbol{\nabla} T + \sum_{k=1}^{N_{\text{g}}} \rho Y_k h_k \boldsymbol{\mathcal{V}}_k + \int \rho Y(v) \mathfrak{h}(v) \boldsymbol{\mathcal{V}}(v)\, \mathrm{d}v \Big) = 0, \tag{1.22}$$

where λ is the global thermal conductivity of the – gas and particles – mixture, h_k is the specific enthalpy of the k^{th} species, $\mathfrak{h}(v)$ is the specific enthalpy of particles whose volume lies in the range $[v, v+\mathrm{d}v]$, and h is the mixture specific enthalpy, given by:

$$h = \sum_{k=1}^{N_{\text{g}}} Y_k h_k + \int Y(v) \mathfrak{h}(v)\, \mathrm{d}v. \tag{1.23}$$

In this work, for the sake of simplicity, we consider the thermal conductivity λ as the thermal conductivity of the pure gas phase. Also, we neglect the Dufour effect, although it could be accounted

for straightforwardly. Note that the mixture specific enthalpy – Equation (1.23) – can be decomposed into a gas and a particle contribution:

$$h = \tilde{h}_{\mathrm{g}} + \tilde{h}_{\mathrm{p}}, \tag{1.24}$$

where $\tilde{h}_{\mathrm{g}}$ and $\tilde{h}_{\mathrm{p}}$ are the respective contributions of the gas and particle phases to the mixture specific enthalpy, which read:

$$\tilde{h}_{\mathrm{g}} = Y_{\mathrm{g}} h_{\mathrm{g}} = \sum_{k=1}^{N_{\mathrm{g}}} Y_k h_k, \tag{1.25}$$

$$\tilde{h}_{\mathrm{p}} = Y_{\mathrm{p}} h_{\mathrm{p}} = \int Y(v) \mathfrak{h}(v) \, \mathrm{d}v, \tag{1.26}$$

$$\tag{1.27}$$

where h_{g} and h_{p} are the gas and particle specific enthapies, respectively.

Finally, the momentum equation reads

$$\frac{\partial(\rho \boldsymbol{u})}{\partial t} + \boldsymbol{\nabla} \cdot (\rho \boldsymbol{u}\boldsymbol{u}) + \boldsymbol{\nabla} p + \boldsymbol{\nabla} \cdot \boldsymbol{\Pi} = 0, \tag{1.28}$$

where p is the pressure and $\boldsymbol{\Pi}$ is the viscous tensor of the – gas and particles – mixture.

When the particle phase is modeled through a pseudo gas component representing the overall nanoparticle mass fraction, then conservations of mass and enthalpy are automatically satisfied as the mixture is reduced to the gas phase.

If the average velocities of the gas and particle phases are not equal, or if the two phases are not in thermal equilibrium, then the two phases must be handled separately, which requires the use of exchange terms. Such a "two-mixture" model is stated in appendix A. It should be noted that, considering for example a nucleation reaction, the enthalpy of the reaction is not in general equal to zero, i.e. the change in chemical energy due to the reaction is generally associated with a change in thermal energy. Therefore, the knowledge of the enthalpy exchange term depends on the reaction considered, and requires the knowledge of energy exchanges at the kinetic level, which is not generaly the case. Akroyd et al. [25] for example write the enthalpy exchange term as:

$$\dot{H}_{\mathrm{gp}} = -\dot{H}_{\mathrm{pg}} = \sum_{k=1}^{N_{\mathrm{g}}} h_k W_k \dot{\omega}_{\mathrm{g},k}^{\mathrm{p}}, \tag{1.29}$$

where $\dot{\omega}_{\mathrm{g},k}^{\mathrm{p}}$ is the molar production rate of the k^{th} gaseous species due to phase change reactions, e.g. nucleation or surface growth. Yet, such assumption is not necessarily true in general. It would be reasonable, indeed, to assume rather that the kinetic energy of the particles is not impacted by the nucleation and/or surface growth processes, so that the change in the particles' enthalpy is only due to chemical variations:

$$\dot{H}_{\mathrm{pg}} = -\dot{H}_{\mathrm{gp}} = \int \mathfrak{h}(v) W(v) \dot{\omega}_{\mathrm{p}}^{\mathrm{g}}(v) \, \mathrm{d}v, \tag{1.30}$$

where $\dot{\omega}_{\mathrm{p}}^{\mathrm{g}}(v)$ is the molar production rate due to phase change reactions – e.g. nucleation or surface growth – of particles whose volume lies in the range $[v, v + \mathrm{d}v]$. Alternatively, one could make the assumption that the net kinetic energy released by the reaction is shared between the two phases according to some empirical ratio [36]. Conversely, in the conservative model proposed here, no exchange terms need to be computed, and the conservation of enthalpy is ensured naturally.

1.2 Discrete formulation

When a sectional model is used, the nanoparticle volume space is no longer continuous but is discretized into a finite number of sections. The conservative model described in subsection 1.1 is easily adapted to a discrete formulation.

In the discrete formulation, the mass density (1.31) of the solid particle mixture reads:

$$\rho_{\mathrm{p}} = \sum_{i=1}^{N_{\mathrm{s}}} \rho_i, \tag{1.31}$$

where N_{s} denotes the number of particle sections, and ρ_i is the i^{th} section density given by:

$$\rho_i = \rho \int_i Y(v)\,\mathrm{d}v, \quad i = 1, \ldots, N_{\mathrm{s}}. \tag{1.32}$$

The integration in Equation 1.32 is over the i^{th} section, i.e. $\int_i \ldots = \int_{v_i^{\min}}^{v_i^{\max}} \ldots$ where $v_i^{\min}$ and $v_i^{\max}$ are the minimum and maximum volumes of the i^{th} section. The i^{th} section nanoparticle mass fraction is then defined as:

$$Y_i = \int_i Y(v)\,\mathrm{d}v = \frac{\rho_i}{\rho}, \quad i = 1, \ldots, N_{\mathrm{s}}. \tag{1.33}$$

The total particle mass fraction reads:

$$Y_{\mathrm{p}} = \sum_{i=1}^{N_{\mathrm{s}}} Y_i = \frac{\rho_{\mathrm{p}}}{\rho} = \frac{\rho_{\mathrm{s}} f_{\mathrm{v}}}{\rho}. \tag{1.34}$$

where f_{v} is the particle volume fraction. The conservation equation for the i^{th} section nanoparticle mass fractions then reads:

$$\frac{\partial(\rho Y_i)}{\partial t} + \boldsymbol{\nabla} \cdot (\rho Y_i \boldsymbol{u} + \rho Y_i \boldsymbol{\mathcal{V}}_i) = \rho_{\mathrm{s}} \dot{Q}_i, \quad i = 1, \ldots, N_{\mathrm{s}}, \tag{1.35}$$

where $\boldsymbol{\mathcal{V}}_i = \int_i Y(v)\boldsymbol{\mathcal{V}}(v)\,\mathrm{d}v / Y_i$ is the diffusion velocity of particles of the i^{th} section, and $\dot{Q}_i = \int_i \dot{q}(v)\,\mathrm{d}v$ (in $\mathrm{cm}^3.\mathrm{cm}^{-3}.\mathrm{s}^{-1}$) is the particle source term for the i^{th} section. For details about the sectional approach, please refer to appendix B.

The mass conservation now reads:

$$\sum_{k=1}^{N_{\mathrm{g}}} W_k \dot{\omega}_k + \sum_{i=1}^{N_{\mathrm{s}}} \rho_{\mathrm{s}} \dot{Q}_i = 0, \tag{1.36}$$

As in the continuous case, the diffusive fluxes must sum to zero:

$$\sum_{k=1}^{N_{\mathrm{g}}} \rho Y_k \boldsymbol{\mathcal{V}}_k + \sum_{i=1}^{N_{\mathrm{s}}} \rho Y_i \boldsymbol{\mathcal{V}}_i = 0, \tag{1.37}$$

so that the constraint (1.11) is satisfied [33]. As well, the mean molar mass of the mixture is now given by

$$\frac{1}{\overline{W}} = \sum_{k=1}^{N_{\mathrm{g}}} \frac{Y_k}{W_k} + \sum_{i=1}^{N_{\mathrm{s}}} \frac{Y_i}{W_i}, \tag{1.38}$$

where W_i is the molar mass of the particles in the i^{th} section – see equation B.6 in appendix B. Note that the system of equations (1.13),(1.14),(1.35) is composed of $N_{\mathrm{g}} + N_{\mathrm{s}} + 1 = N + 1$ formally

independent unknowns, where N is the total number of mixture components, but because of the implicit constraint (1.11) there are only N physically-independent unknowns, as expected.

In the present work, the diffusion velocities of the gas-phase species and nanoparticles are given by:

$$\boldsymbol{\mathcal{V}}_k = -D_k \boldsymbol{\nabla} \ln X_k + \boldsymbol{u}_{\rm cor}, \tag{1.39}$$

$$\boldsymbol{\mathcal{V}}_i = \boldsymbol{v}_{\rm th} - D_i \boldsymbol{\nabla} \ln Y_i + \boldsymbol{u}_{\rm cor}. \tag{1.40}$$

The diffusion coefficient of particles of the $i^{\rm th}$ section has been assumed constant $D(v) \simeq D_i$ over each section. The correction velocity $\boldsymbol{u}_{\rm cor}$ is adjusted to satisfy the constraint (1.37).

When the nanoparticle concentration is low, only the gaseous species diffusion velocities are generally corrected, namely:

$$\boldsymbol{\mathcal{V}}_k = -D_k \boldsymbol{\nabla} \ln X_k + \boldsymbol{u}^{\rm g}_{\rm cor}, \tag{1.41}$$

$$\sum_{k=1}^{N_{\rm g}} Y_k \boldsymbol{\mathcal{V}}_k = 0. \tag{1.42}$$

where $\boldsymbol{u}^{\rm g}_{\rm cor}$ is a correction velocity adjusted to satisfy the constraint (1.42).

If the latter model is used for highly concentrated aerosols, one obtains a non-conservative set of equations potentially leading to large errors or numerical instabilities. In the following, this "non-mass-conserving" formulation will be compared to the conservative formulation (1.39)-(1.40).

The mixture specific enthalpy is now given by

$$h = \sum_{k=1}^{N_{\rm g}} Y_k h_k + \sum_{i=1}^{N_{\rm s}} Y_i h_i. \tag{1.43}$$

where h_i is the average specific enthalpy of particles in the $i^{\rm th}$ section. The – isobaric – mixture enthalpy conservation equation can be written as:

$$\frac{\partial(\rho h)}{\partial t} + \boldsymbol{\nabla} \cdot (\rho h \boldsymbol{u}) + \boldsymbol{\nabla} \cdot \Big(- \lambda \boldsymbol{\nabla} T + \sum_{k=1}^{N_{\rm g}} \rho Y_k h_k \boldsymbol{\mathcal{V}}_k + \sum_{i=1}^{N_{\rm s}} \rho Y_i h_i \boldsymbol{\mathcal{V}}_i \Big) = 0. \tag{1.44}$$

In particular, the contribution of the particle phase to the mixture specific enthalpy reads:

$$\tilde{h}_{\rm p} = Y_{\rm p} h_{\rm p} = \sum_{i=1}^{N_{\rm s}} Y_i h_i. \tag{1.45}$$

It should be reminded that in classical models of fine particles, when the nanoparticle concentration is low, generally the mixture specific enthalpy is computed as:

$$h = \sum_{k=1}^{N_{\rm g}} Y_k h_k, \tag{1.46}$$

and the contribution of the nanoparticles $\sum_{i=1}^{N_{\rm s}} \rho Y_i h_i \boldsymbol{\mathcal{V}}_i$ to the heat flux is neglected in equation (1.44). In the present work, this "non-energy-conserving" formulation will be compared to the conservative formulation (1.43)-(1.44).

Finally, the momentum equation (1.28) remains unchanged in the discrete case.

2 Titania synthesis in flames

In order to demonstrate the importance of a conservative formulation, the synthesis of titania nanoparticles is considered here as a case illustration. Any other kinds of fine particles that can be produced in flames could be addressed. As the main purpose of this article is to demonstrate the importance of conservation of mass and energy, the nucleation kinetics is simplified to a one-step nucleation model, which is such that nucleation is a complete and fast reaction. Such a model represents well the rapidity of the nucleation process, without fine details on the actually followed nucleation pathways.

Physical processes involved – nucleation, coagulation, and surface growth – are described in this section. No sintering is considered since the shape of the nanoparticles produced is not relevant for the purpose of the present study. The source term $\dot{Q}_i$ (in s^{-1}) in Equation (1.35) thus reads:

$$\dot{Q}_i = \dot{Q}_{\mathrm{nu},i} + \dot{Q}_{\mathrm{coag},i} + \dot{Q}_{\mathrm{sg},i}. \tag{2.1}$$

2.1 Nucleation model

One of the main precursors used in industrial processes for flame synthesis of TiO_2 nanoparticles is titanium tetrachloride ($TiCl_4$). Pratsinis et al. [8] first described the oxidation of $TiCl_4$ vapor between 700 and 1000°C as a one-step chemical reaction:

$$\mathrm{TiCl_4(g) + O_2(g) \rightarrow TiO_2(s) + 2Cl_2(g)} \tag{2.2}$$

The rate is first-order with respect to $TiCl_4$, and nearly zeroth-order for O_2 up to a 10-fold oxygen excess. Accordingly, the titania nanoparticle nucleation rate can be written in the following form [8,14]:

$$\dot{Q}_{\mathrm{nu},i} = \delta_{i1}\, \max\left(0, \mathcal{K}_{\mathrm{1step}} n_{\mathrm{TiCl_4}} - \mathcal{K}_{\mathrm{sg}}\, A_{\mathrm{p}}\right) v_{\mathrm{TiO_2}}, \tag{2.3}$$

where δ_{i1} equals 1 if $i = 1$ and 0 otherwise, $n_{\mathrm{TiCl_4}}$ is the $TiCl_4$ number density (cm^{-3}), $v_{\mathrm{TiO_2}}$ is the volume of a monomer (cm^3), $\mathcal{K}_{\mathrm{1step}}$ (in s^{-1}) is the one-step rate constant, $\mathcal{K}_{\mathrm{sg}}$ (in $\mathrm{cm}^{-2}.\mathrm{s}^{-1}$) is the surface growth rate, and A_{p} ($\mathrm{cm}^2.\mathrm{cm}^{-3}$) is the particle surface area concentration, in our case equal to:

$$A_{\mathrm{p}} = \int_0^\infty s(v) n(v)\, \mathrm{d}v, \tag{2.4}$$

with $s(v)$ (in cm^2) the surface of a nanoparticle of volume v, and $n(v) = q(v)/v$ (in cm^{-3}) the particle number density.

The one-step rate constant reads:

$$\mathcal{K}_{\mathrm{1step}} = 8.26 \cdot 10^4 \exp\left(-\mathfrak{E}_{\mathrm{1step}}/(RT)\right) \tag{2.5}$$

with $\mathfrak{E}_{\mathrm{1step}} = 88.8$ kJ.mol^{-1} the activation energy and T the gas temperature. This rate has been the basis of many numerical studies of TiO_2 nanoparticle formation [9,14–17,26,37]. When surface growth is taken into account, the nucleation rate must be adjusted as in Equation (2.3) so that the total number of $TiCl_4$ molecules consumed is equal to the sum of the nucleation rate and the surface growth rate [16,20]. The expression for the surface growth rate will be detailed in section 2.3.

As the purpose of this paper is essentially to demonstrate the importance of using a conservative set of equations, the one-step nucleation scheme is adopted here in conjunction with GRI-Mech 3.0 [38] for the oxidation of methane. Following the recommandations of Mehta et al. [20], we consider the nucleated particles to contain five Ti atoms. In other words, the smallest volume of the first section is taken equal to $v_1^{\min} = 5\, v_{\mathrm{TiO_2}}$. The thermodynamic and transport data for $TiCl_4$, Cl_2 and TiO_2 are taken from [39]. The density of titania nanoparticles is assumed constant, equal to $\rho_{\mathrm{s}} = 4000$ kg.m^{-3} [14].

2.2 Coagulation

The global coagulation source term is expressed according to Smoluchowski's expression [40]:

$$\dot{Q}_{\mathrm{coag},i} = \left(\sum_{1\leq j\leq k}^{i} \dot{N}_{coag}^{j,k\to i} - \sum_{j=1}^{N_\mathrm{s}} \dot{N}_{ij}^{\mathrm{out}} \right) \frac{Q_i}{N_i} = \left(\sum_{1\leq j\leq k}^{i} \dot{N}_{coag}^{j,k\to i} - \sum_{j=1}^{N_\mathrm{s}} \dot{N}_{ij}^{\mathrm{out}} \right) \frac{\left(v_i^{\max} - v_i^{\min}\right)}{\ln\left(\frac{v_i^{\max}}{v_i^{\min}}\right)}. \tag{2.6}$$

$\dot{N}_{\mathrm{coag}}^{j,k\to i}$ is the number of particles received by the i^{th} section due to collisions of particles from the j^{th} and k^{th} sections per unit time:

$$\dot{N}_{\mathrm{coag}}^{j,k\to i} = \left(1 - \frac{\delta_{jk}}{2}\right) \iint\limits_{v+w\in[v_i^{\min},v_i^{\max}]} \beta_{j,k} n_j(v) n_k(w)\, dvdw \tag{2.7}$$

The factor $\frac{1}{2}$ is required when $j = k$ to avoid counting twice the same colliding pair [41]. $\dot{N}_{ij}^{\mathrm{out}}$ is the number of particles leaving the i^{th} section upon collision with particles of the j^{th} section per unit time:

$$\dot{N}_{ij}^{\mathrm{out}} = \int_{v_i^{\min}}^{v_i^{\max}} \int_{v_j^{\min}}^{v_j^{\max}} \beta_{i,j} n_i(v) n_j(w)\, dvdw \tag{2.8}$$

The collision frequency $\beta_{i,j}$ between a particle of the i^{th} section and a particle of the j^{th} section is evaluated at v_i^{mean} and v_j^{mean}. Here, a transition regime between the free molecular regime (superscript $^{\mathrm{fm}}$) and the continuum regime (superscript $^{\mathrm{c}}$) has been chosen for the description of collisions, so that $\beta_{i,j}$ is expressed as:

$$\beta_{i,j} = \frac{\beta_{i,j}^{\mathrm{fm}} \beta_{i,j}^{\mathrm{c}}}{\beta_{i,j}^{\mathrm{fm}} + \beta_{i,j}^{\mathrm{c}}} \approx \min(\beta_{i,j}^{\mathrm{fm}}, \beta_{i,j}^{\mathrm{c}}) \tag{2.9}$$

with:

$$\begin{aligned} \beta_{i,j}^{\mathrm{fm}} = &\ \frac{1}{2}\,\epsilon_{\mathrm{coag}} \left(\frac{2\pi k_b T}{\rho_\mathrm{s}}\right)^{1/2} \sqrt{\frac{1}{v_i^{\mathrm{mean}}} + \frac{1}{v_j^{\mathrm{mean}}}} (d_{c,i} + d_{c,j})^2 \\ \beta_{i,j}^{\mathrm{c}} = &\ \frac{2k_b T}{3\mu} (d_{c,i} + d_{c,j}) \left(\frac{\mathrm{C}_i}{d_{c,i}} + \frac{\mathrm{C}_j}{d_{c,j}}\right) \end{aligned} \tag{2.10}$$

where $\epsilon_{\mathrm{coag}} = 2.2$ is an amplification factor due to Van der Waals interactions [42,43] and μ is the gas dynamic viscosity given by Sutherland's formula [44] $\mu = C_1 T^{3/2}/(T + C_2)$. The coefficients C_1 and C_2 are the Sutherland coefficients, and C_j is the Cunningham corrective coefficient for a particle of the j^{th} section [45,46]:

$$\mathrm{C}_j = 1 + 1.257\,\mathrm{Kn}_j = 1 + 1.257\,\frac{2l_{\mathrm{gas}}}{d_{c,j}} \tag{2.11}$$

where Kn_j is the Knudsen number, and $d_{c,j}$ is the collisional diameter of a particle of the j^{th} section, considered constant and evaluated as a function of n_j, d_j and the fractal dimension D_f of particles:

$$d_{c,j} = d_j n_j^{1/D_f}. \tag{2.12}$$

Finally, l_{gas} is the mean free path of the gaseous phase, expressed by:

$$l_{\mathrm{gas}} = \frac{k_b T}{\sqrt{2}\pi d_{\mathrm{gas}}^2 p}, \tag{2.13}$$

where k_b, T, $d_{\mathrm{gas}} = 0.2$ nm, and p correspond respectively to the Boltzmann constant, the temperature, the diameter of a typical gas particle and the pressure. As we consider here spherical particles, the fractal dimension D_f is equal to 1 and $d_{c,j} = d_j$.

2.3 Surface growth

Particles interact at their surface with the surrounding species in the gas phase. Surface growth leads to an increase of the particle size. The surface growth source term for the i^{th} section reads:

$$\dot{Q}_{\text{sg},i} = \dot{Q}_{\text{sg},i}^{i\to i} + \dot{Q}_{\text{sg},i}^{i-1\to i} - \dot{Q}_{\text{sg},i}^{i\to i+1}, \tag{2.14}$$

where $\dot{Q}_{\text{sg},i}^{i\to i}$, $\dot{Q}_{\text{sg}}^{i-1\to i}$ and $\dot{Q}_{\text{sg}}^{i\to i+1}$ respectively correspond to the amount of mass of gaseous species that will condensate on particles of the i^{th} section, to the amount of particle mass that will enter into the i^{th} section due to deposition on particles of the section $i-1$, and to the amount of particle mass that will move from the i^{th} section to section $i+1$ due to surface growth.

The rates $\dot{Q}_{\text{sg},i}^{i\to i}$, $\dot{Q}_{\text{sg},i}^{i-1\to i}$ and $\dot{Q}_{\text{sg},i}^{i\to i+1}$ can be expressed as [43]:

$$\begin{aligned}
\dot{Q}_{\text{sg},i}^{i\to i} &= \int_{v_i^{\min}}^{v_i^{\max}-v_{\text{TiO}_2}} \mathcal{K}_{\text{sg}}\, s(w)\, n(w)\, v_{\text{TiO}_2}\, dw \\
\dot{Q}_{\text{sg},i}^{i-1\to i} &= \int_{v_{i-1}^{\max}-v_{\text{TiO}_2}}^{v_{i-1}^{\max}} \mathcal{K}_{\text{sg}}\, s(w)\, n(w)\, (w+v_{\text{TiO}_2})\, dw \\
\dot{Q}_{\text{sg},i}^{i\to i+1} &= \int_{v_i^{\max}-v_{\text{TiO}_2}}^{v_i^{\max}} \mathcal{K}_{\text{sg}}\, s(w)\, n(w)\, w\, dw
\end{aligned} \tag{2.15}$$

where $\mathcal{K}_{\text{sg}}$ is the reaction constant obtained from the surface growth mechanism.

The surface growth proceeds from $TiCl_4$ oxidation. We use the surface growth model of Ghoshtagore et al. [47], namely the reaction:

$$TiCl_4(g) + O_2(g) \xrightarrow{\text{surface}} TiO_2(s) + 2Cl_2(g), \tag{2.16}$$

assumed irreversible with a forward rate given in $\text{cm}^{-2}.\text{s}^{-1}$ by:

$$\mathcal{K}_{\text{sg}} = k_{\text{s}}(T)\, n_{TiCl_4}, \tag{2.17}$$

where k_{s} (cm.s^{-1}) reads:

$$k_{\text{s}}(T) = 4,9 \cdot 10^3 \exp\Big(-\frac{\mathfrak{E}_{\text{s}}}{RT}\Big) \tag{2.18}$$

with $\mathfrak{E}_{\text{s}} = 74.8$ kJ.mol^{-1}. This reaction rate was estimated by Ghoshtagore and coworkers from experimental measurements at 673-1020 K [47], and has been used in many numerical studies [14–17].

3 Results in 1D premixed configuration

Here we analyze the importance of respecting the conservation of enthalpy when high concentrations of TiO_2 are encountered in the reactive flow. One-dimensional (1D) premixed $CH_4/TiCl_4/O_2/N_2$ flames are calculated using the 1D premixed model in the in-house code Regath [43,48]. In the configuration studied here, the low Mach number approximation applies and the momentum equation is not needed. The corresponding equations are stated in appendix C. The CH_4/O_2 mixture is at stoichiometric conditions. The $TiCl_4$ inlet mass fraction is equal to 5 %, the O_2 inlet mass fraction is 22.0 % and the N_2 mass fraction is 67.5 %.

Figures 1a and 1b show respectively the main combustion species mass fraction and temperature profiles, and the $TiCl_4$, Cl_2 and TiO_2 mole fraction profiles in the 1D premixed flame. Although the mass fractions are generally the variables of interest, as they are the transported variables, in the present case the Ti-containing species mole fractions are plotted rather than the mass fractions, as the number of Ti atoms is conserved so that the conversion yield can be visualized more easily

in terms of mole fractions. As it can be seen in Figure 1b, the conversion of $TiCl_4$ into TiO_2 is very efficient, almost equal to 100%. The TiO_2 one-step reaction is relatively fast, although the reaction front is much less stiff than the combustion front depicted in Figure 1a. With such a high nanoparticle concentration, it is expected that the phase change has some impact on the gas-phase enthalpy, and therefore on the flame structure.

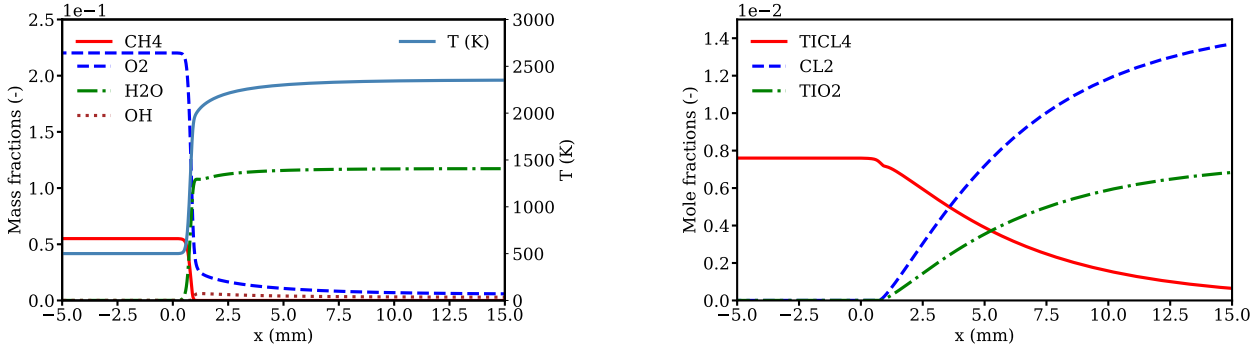

(a) Main species mass fractions and temperature.

(b) Titania species mole fractions.

Figure 1 – Main species and temperature profiles for the 1D premixed $CH_4/O_2/N_2$ flame at stoichiometric conditions. The inlet temperature is 500 K. Injected $TiCl_4$ mass fraction $Y^{\text{inj}}_{TiCl_4} = 5 \cdot 10^{-2}$.

In Figure 2 the enthalpies of the respective phases – gas/particle – and the enthalpy of the mixture are plotted. The absolute value of the gas enthalpy $\tilde{h}_g$ decreases significantly as the $TiCl_4$ is converted into TiO_2. In the burnt gases, most of the mixture enthalpy h comes from the particle enthalpy $\tilde{h}_p$, even though the injected mass fraction of $TiCl_4$ is only 5%. This is due to the relatively large absolute value of the enthalpy of TiO_2 [49].

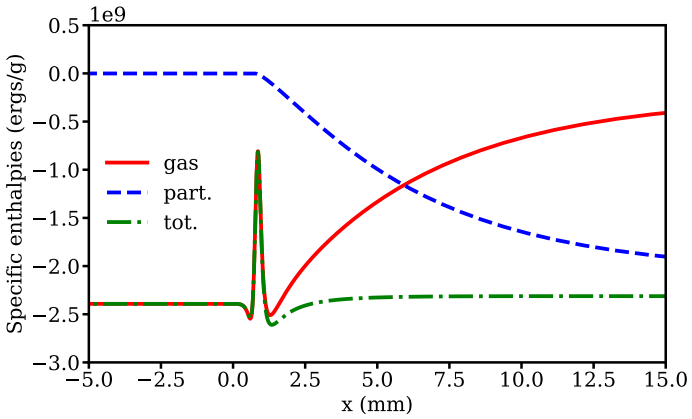

Figure 2 – Enthalpies of the gas phase $\tilde{h}_g$, the solid particle phase $\tilde{h}_p$, and the mixture h. Same conditions as in Figure 1.

In Figure 3 the temperature profile obtained with the energy-conserving model – equations (1.22)-(1.23) and (1.43)-(1.44) – is compared with the one obtained using the non-energy-conserving formulation – generally used for fine particles when the concentration is low – where the contribution of the nanoparticles to the enthalpy is neglected – equation (1.46). As expected the flame structure

is significantly impacted. For only 5% of $TiCl_4$, the adiabatic temperature is increased by 95 K when the conservative model is used compared to the non-conservative formulation. For higher injection rate typical of industrial conditions the effect is expected to be even higher. If one neglects the enthalpy of the particle phase in equations (1.22)-(1.23) and (1.43)-(1.44), then the set of equations is non-conservative in essence and yields non-physical results. Indeed, exchanges of enthalpy occur between the gas and the particle phases, and thus neglecting $\tilde{h}_{\mathrm{p}}$ yields for instance an erroneous temperature in the burnt gases.

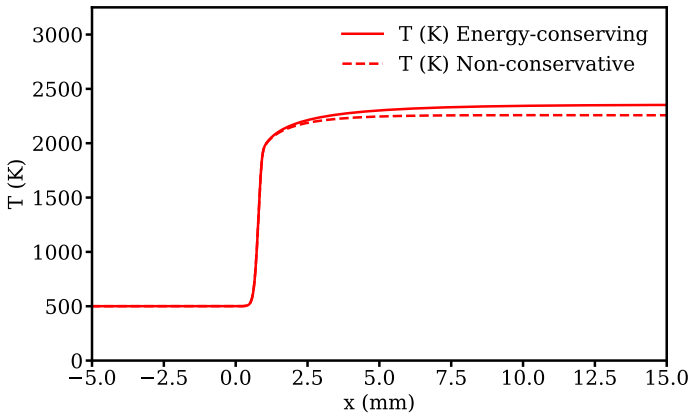

Figure 3 – Comparison of the temperature profiles obtained with the energy-conserving model and the non-energy-conserving one. Same conditions as in Figures 1.

In addition, neglecting the enthalpy of the particles can lead to severe numerical difficulties. The numerical method used for the present study is fully coupled. The set of discretized equations is solved by means of a modified Newton method. Therefore, the conservation of energy is critical. When neglecting the particle enthalpy h_{p}, as earlier authors did, we could not obtain numerical convergence when $TiCl_4$ injected mass fraction was greater than 5%, even though continuation techniques were employed. The system seems to become singular when the nanoparticle mass fraction becomes too large. This is due to the fact that with an implicit method when using the conservative model the condition $h(+\infty) = h(-\infty)$ is enforced. On the contrary, when neglecting $\tilde{h}_{\mathrm{p}}$, the condition $\tilde{h}_{\mathrm{g}}(+\infty) = \tilde{h}_{\mathrm{g}}(-\infty)$ is imposed, which is not possible. If one uses an explicit or semi-implicit solver, such numerical difficulty is circumvented, but the system of equations used is still non-conservative and may lead to converged but non-physical solutions.

In premixed configurations diffusion of nanoparticles is relatively negligible as the mixture rapidly reaches a thermodynamic equilibrium, especially here given the fast $TiCl_4$ conversion rates, so that the computation of the diffusion velocity is not critical. However, in non-premixed counterflow configurations, relative diffusion due to concentration gradients and thermophoresis can play an important role in the flame and nanoparticle dynamics, as discussed in the following section.

4 Results in 1D non-premixed counterflow configuration

In this section, we study first the importance of enthalpy conservation, then the importance of differential diffusion with respect to mass conservation. 1D counterflow non-premixed flames are calculated using the 1D counterflow model in the Regath code [43,48]. In the configuration studied here, the low Mach number approximation applies and the corresponding equations are stated in appendix D.

4.1 Enthalpy conservation

We investigate here the importance of the global conservation of mass and enthalpy in the mixture in a CH_4/O_2 diffusion flame. Figure 4 shows results for a counterflow CH_4/O_2+$TiCl_4$ flame. The oxidizer mixture is injected from the left, and contains 25 % $TiCl_4$ and 75 % O_2 in mass, while the – 100 % CH_4 – fuel is injected from the right. The injection temperature is of 500 K on both sides, and the strain rate is $600\,s^{-1}$. The origin is set at the stagnation plane.

In Figure 4a, respectively Figure 4b, the main combustion species mass fraction and temperature profiles, respectively the titania species mole fraction profiles, are plotted. It can be seen that the maximum temperature and H_2O mass fraction – Figure 4a – are located on the oxidizer side due to high diffusion of CH_4. The $TiCl_4$ conversion into TiO_2 – Figure 4b – is almost completed at maximum temperature while TiO_2 is formed as soon as H_2O mass fraction increases. The TiO_2 mole fraction has a non-linear behavior near the stagnation point because of the intricate effect of convection and thermophoresis. Indeed, the convection decreases as the nanoparticles get closer to the stagnation plane, while the thermophoretic force is first directed upstream of the flow, turns downstream as the nanoparticles cross the maximum temperature point, and increases as the nanoparticles cross the zone of maximum temperature gradient.

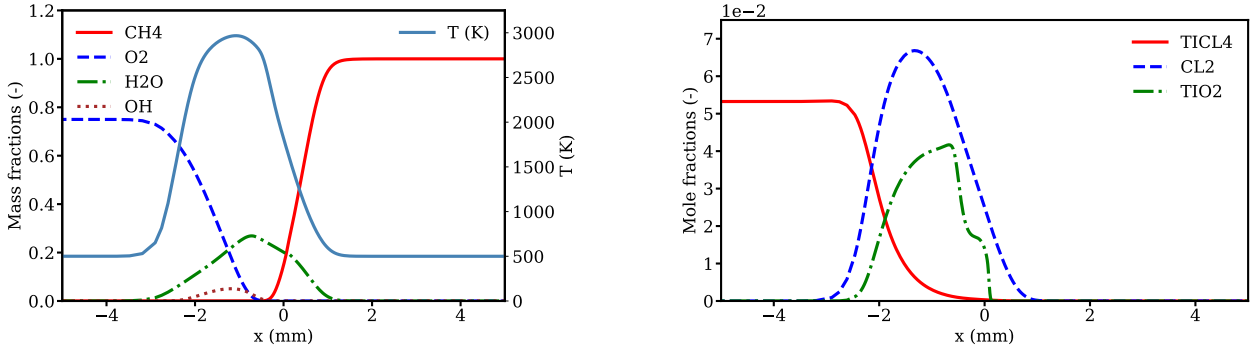

(a) Main species mass fractions and temperature.

(b) Titania species mole fractions.

Figure 4 – Main species sprofiles for the 1D counterflow CH_4/O_2 flame. The inlet temperature is 500 K. Injected $TiCl_4$ mass fraction $Y^{\text{inj}}_{TiCl_4} = 0.25$ (oxidizer side). Strain rate $\alpha = 600\,s^{-1}$. The stagnation plane is located at $x = 0\,\text{mm}$.

In Figure 5, the enthalpies of the respective gas and particle phases are plotted for the 1D counterflow flame of Figure 4a. As in the premixed case, one can see that the enthalpy of the particle phase represents a non-negligible part of the enthalpy of the mixture in the counterflow flame. However, a much higher injected $TiCl_4$ mass fraction – 25 %‘ – is necessary compared to the premixed case – 5 % – to observe a comparable relative contribution of TiO_2 enthalpy to the mixture enthalpy. This is because the absolute value of CH_4 specific enthalpy at 500 K is one order of magnitude larger than the specific enthalpies of O_2 and N_2, so that the relative contribution of TiO_2 appears lower, although the absolute contribution in the counterflow flame – $\sim -10^{10}$ at 25 % $TiCl_4$ – is consistent with that observed in the premixed flame – $\sim -2 \cdot 10^9$ at 5 % $TiCl_4$.

It is worth noting that no convergence issues were encountered for this configuration when using the non-energy-conserving model. Indeed, while in the premixed flame the boundary conditions are constrained by the conservation of total enthalpy, in the counterflow flame no such constraint exists owing to the lateral heat loss.

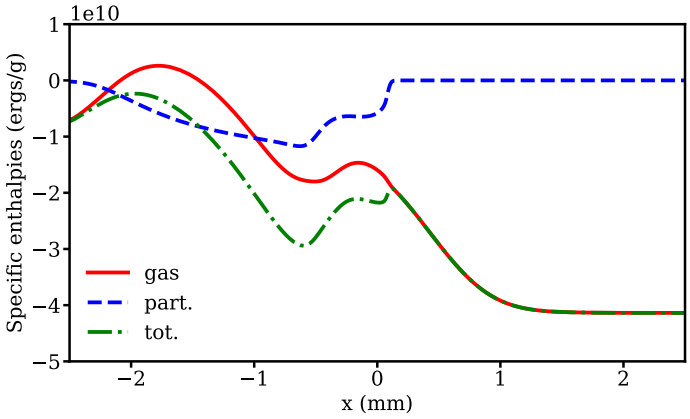

Figure 5 – Respective contributions $\tilde{h}_{\mathrm{g}}$ and $\tilde{h}_{\mathrm{p}}$ of the gas and solid particle phases to the mixture specific enthalpy h. Same conditions as in Figure 4.

4.2 Mass conservation

In 1D premixed configurations, the diffusion of particles plays a negligible role, while in counterflow flames we expect a more significant impact. To assess this impact, we run two calculations. In the first calculation, we use the conservative model, where the correction velocity is adjusted so that the diffusive fluxes of both gaseous species and particles sum to zero, as in equations (1.39)-(1.40). This model is referred to as the "mass-conserving" model. In a second calculation, the contribution of nanoparticles to the correction velocity is neglected, and only the gaseous species diffusion velocities are corrected, as in equations (1.41)-(1.42). Figure 6 presents the comparison between the two calculations. The differences in titania mole fractions are not negligible between the two cases. When the conservative model is used, the maximum mole fraction of TiO_2 is higher than when the non-conservative model is used. With the latter model, more nanoparticles cross the stagnation plane than with the conservative model, probably because thermophoresis is hindered by neutral drag. However, the effect on the flame structure appears negligible. Indeed, the temperature profiles – not shown here – are almost identical. Only the combustion products are affected in the area where nanoparticles are present: the H_2O, CO and CO_2 mass fraction profiles, plotted in Figure 6b, are very similar, excepted that the non-conservative model leads to the apparition of a local maximum in the H_2O and CO_2 profile close to the stagnation plane, and a shift in the CO maximum mole fraction towards the stagnation plane. However, disposing of a conservative formulation in terms of both mass and enthalpy is essential to guarantee the physical consistency of the results.

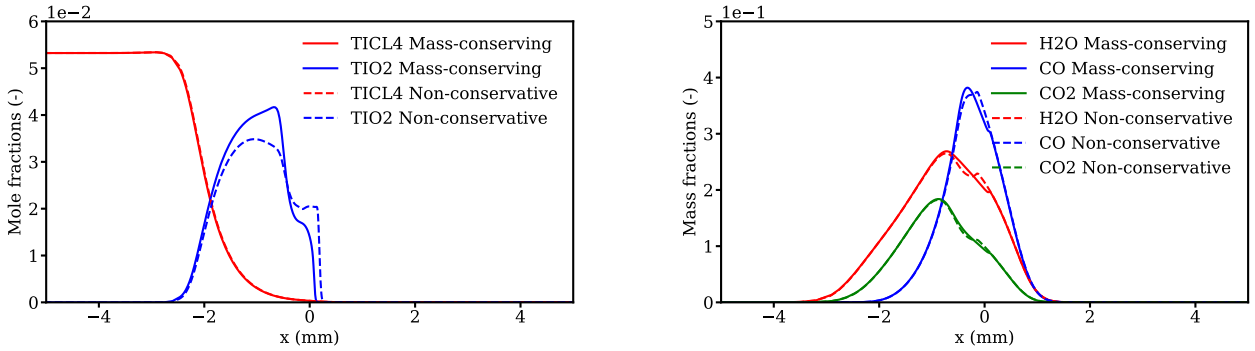

(a) $TiCl_4$ and TiO_2 mole fraction profiles.

(b) Mass fraction profiles of H_2O, CO and CO_2.

Figure 6 – Comparison between the mass-conserving and the non-conservative formulations in the counterflow flame. Same conditions as in Figure 4.

5 Conclusion

In this work, we have studied the modeling of nanoparticle production in a reactive flow at a high concentration. First, it has been shown that the conservation of enthalpy and mass is of great importance, both for numerical stability and physical consistency purposes. The relative importance of the particle-phase enthalpy has been illustrated both in 1D premixed and in 1D counterflow calculations. It has been shown that the enthalpy of the particle phase can represent a significant part of the mixture enthalpy, which cannot be neglected, as traditionally done in soot or fine particle models. Besides, using a non-enthalpy-conserving scheme may lead to severe numerical difficulties, at least when an implicit scheme is used.

Second, the importance of differential diffusion has been demonstrated in 1D counterflow simulations. Even though the particles diffuse slower than the gaseous species, the conservation of mass requires to account for a correction velocity due to thermophoresis. Neglecting this term can have a strong influence on the nanoparticle volume fraction profile, notably in counterflow flames. Contrary to enthalpy conservation, no numerical instabilities have been observed due to non-conservation of mass. The results show a non-negligible effect of non conserving the mass, although the effect is less pronounced than in the case of enthalpy. The proposed conservative formulation represents a well-based mathematical framework for the numerical investigation of high-yield flame synthesis of nanoparticles.

Acknowledgments

The support of the European Research Council (ERC) under the European Union Horizon 2020 research and innovation programme (grant agreement No. 757912) is acknowledged.

A Two-mixture model

Alternatively to the one-mixture formulation proposed in this work, a two-mixture model can be considered. In the two-mixture model, one solves the balance equations for the gas-phase and particle-phase densities, ρ_g, ρ_p, respectively. Then one solves equations for the gaseous species and

particles mass fractions in each phase separately, respectively defined as:

$$\begin{aligned} Y_k^{\mathrm{g}} &= \frac{\rho_k}{\rho_{\mathrm{g}}}, \quad k = 1, \ldots, N_{\mathrm{g}}, \\ Y^{\mathrm{p}}(v)\,\mathrm{d}v &= \frac{\rho_{\mathrm{s}}\, q(v)}{\rho_{\mathrm{p}}}\,\mathrm{d}v. \end{aligned} \tag{A.1}$$

where N_{g} is the number of gas-phase species, ρ_k is the density of the k^{th} gaseous species and $q(v)$ is the volume density of the aerosol. In this formalism, the two following separate mass constraints must then be satisfied:

$$\begin{aligned} \sum_{k=1}^{N_{\mathrm{g}}} Y_k^{\mathrm{g}} &= 1, \\ \int Y^{\mathrm{p}}(v)\,\mathrm{d}v &= 1. \end{aligned} \tag{A.2}$$

We also define the global gaseous and particle mass fractions, respectively by:

$$\begin{aligned} Y_{\mathrm{g}} &= \frac{\rho_{\mathrm{g}}}{\rho}, \\ Y_{\mathrm{p}} &= \frac{\rho_{\mathrm{p}}}{\rho}, \end{aligned} \tag{A.3}$$

where ρ is the mixture density. These global mass fractions also sum to unity:

$$Y_{\mathrm{g}} + Y_{\mathrm{p}} = 1. \tag{A.4}$$

As a matter of generality, we do not assume here that the velocities of the gas and particle phases $\boldsymbol{u}_{\mathrm{g}}$ and $\boldsymbol{u}_{\mathrm{p}}$ are equal. The mixture-averaged velocity $\boldsymbol{u}$ is then given by:

$$\rho \boldsymbol{u} = \rho_{\mathrm{g}} \boldsymbol{u}_{\mathrm{g}} + \rho_{\mathrm{p}} \boldsymbol{u}_{\mathrm{p}}. \tag{A.5}$$

Therefore, one ends up with the following system of balance equations for the two-phase multicomponent flow:

$$\frac{\partial \rho}{\partial t} + \boldsymbol{\nabla} \cdot (\rho \boldsymbol{u}) = 0, \tag{A.6}$$

$$\frac{\partial \rho_{\mathrm{g}}}{\partial t} + \boldsymbol{\nabla} \cdot (\rho_{\mathrm{g}} \boldsymbol{u}_{\mathrm{g}}) = \sum_{k=1}^{N_{\mathrm{g}}} W_k \dot{\omega}_k, \tag{A.7}$$

$$\frac{\partial \rho_{\mathrm{p}}}{\partial t} + \boldsymbol{\nabla} \cdot (\rho_{\mathrm{p}} \boldsymbol{u}_{\mathrm{p}}) = \int \rho_{\mathrm{s}}\, \dot{q}(v)\,\mathrm{d}v, \tag{A.8}$$

$$\frac{\partial (\rho_{\mathrm{g}} Y_k^{\mathrm{g}})}{\partial t} + \boldsymbol{\nabla} \cdot (\rho_{\mathrm{g}} Y_k^{\mathrm{g}} \boldsymbol{u}_{\mathrm{g}} + \rho_{\mathrm{g}} Y_k^{\mathrm{g}} \boldsymbol{\mathcal{V}}_k^{\mathrm{g}}) = W_k \dot{\omega}_k, \quad k = 1, \ldots, N_{\mathrm{g}}, \tag{A.9}$$

$$\frac{\partial (\rho_{\mathrm{p}} Y^{\mathrm{p}}(v))}{\partial t} + \boldsymbol{\nabla} \cdot (\rho_{\mathrm{p}} Y^{\mathrm{p}}(v) \boldsymbol{u}_{\mathrm{p}} + \rho_{\mathrm{p}} Y^{\mathrm{p}}(v) \boldsymbol{\mathcal{V}}^{\mathrm{p}}(v)) = \rho_{\mathrm{s}}\, \dot{q}(v), v \in]0, +\infty[. \tag{A.10}$$

In these equations, $\boldsymbol{\mathcal{V}}_k^{\mathrm{g}}$ is the diffusion velocity of the k^{th} species in the gas reference frame and $\boldsymbol{\mathcal{V}}^{\mathrm{p}}(v)$ is the diffusion velocity of particles whose volume lies in the range $[v, v + \mathrm{d}v]$ with respect to the particles reference frame. The diffusion velocities are adjusted to satisfy the mass conservation constraints:

$$\begin{aligned} \sum_{k=1}^{N_{\mathrm{g}}} \rho_{\mathrm{g}} Y_k^{\mathrm{g}} \boldsymbol{\mathcal{V}}_k^{\mathrm{g}} &= 0, \\ \int \rho_{\mathrm{p}} Y^{\mathrm{p}}(v) \boldsymbol{\mathcal{V}}^{\mathrm{p}}(v)\,\mathrm{d}v &= 0. \end{aligned} \tag{A.11}$$

The mixture density ρ is still given by the perfect gas law (1.18). The average molar mass is now obtained from:

$$\frac{1}{\overline{W}} = \frac{Y_\mathrm{g}}{\overline{W}_\mathrm{g}} + \frac{Y_\mathrm{p}}{\overline{W}_\mathrm{p}}, \tag{A.12}$$

where $\overline{W}_\mathrm{g}$ and $\overline{W}_\mathrm{p}$ are the mean molar mass of the gas and particle phases, respectively:

$$\begin{aligned} \frac{1}{\overline{W}_\mathrm{g}} &= \sum_{k=1}^{N_\mathrm{g}} \frac{Y_k^\mathrm{g}}{W_k}, \\ \frac{1}{\overline{W}_\mathrm{p}} &= \int \frac{Y^\mathrm{p}(v)}{W(v)}\,\mathrm{d}v, \end{aligned} \tag{A.13}$$

where $W(v)$ is the molar mass of the particles whose volume lies in the range $[v, v+\mathrm{d}v]$.

As the two phases are not in momentum equilibrium, two separate balance equations are then required for $\boldsymbol{u}_\mathrm{g}$ and $\boldsymbol{u}_\mathrm{p}$, namely:

$$\frac{\partial(\rho_\mathrm{g}\boldsymbol{u}_\mathrm{g})}{\partial t} + \boldsymbol{\nabla}\cdot(\rho_\mathrm{g}\boldsymbol{u}_\mathrm{g}\boldsymbol{u}_\mathrm{g} + p_\mathrm{g}\mathbb{I}) + \boldsymbol{\nabla}\cdot\boldsymbol{\Pi}_\mathrm{g} = \boldsymbol{F}_\mathrm{gp}, \tag{A.14}$$

$$\frac{\partial(\rho_\mathrm{p}\boldsymbol{u}_\mathrm{p})}{\partial t} + \boldsymbol{\nabla}\cdot(\rho_\mathrm{p}\boldsymbol{u}_\mathrm{p}\boldsymbol{u}_\mathrm{p} + p_\mathrm{p}\mathbb{I}) + \boldsymbol{\nabla}\cdot\boldsymbol{\Pi}_\mathrm{p} = \boldsymbol{F}_\mathrm{pg}, \tag{A.15}$$

where p_g, p_p are the gas and particle partial pressures, respectively, $\boldsymbol{\Pi}_\mathrm{g}$ and $\boldsymbol{\Pi}_\mathrm{p}$ are the gas and particle viscous tensors, respectively, and $\boldsymbol{F}_\mathrm{gp} = -\boldsymbol{F}_\mathrm{pg}$ is the force exerted by the particle phase on the gas phase.

In order to complete the above set of balance equations, one should also account for the conservation of enthalpy. In the two-mixture model, the balance equations for the gas and particle enthalpies read:

$$\frac{\partial(\rho_\mathrm{g}h_\mathrm{g})}{\partial t} + \boldsymbol{\nabla}\cdot(\rho_\mathrm{g}h_\mathrm{g}\boldsymbol{u}_\mathrm{g}) + \boldsymbol{\nabla}\cdot\Big(-\lambda_\mathrm{g}\boldsymbol{\nabla}T_\mathrm{g} + \sum_{k=1}^{N_\mathrm{g}}\rho_\mathrm{g}Y_k^\mathrm{g}h_k\boldsymbol{\mathcal{V}}_k^\mathrm{g}\Big) = \dot{H}_\mathrm{gp}, \tag{A.16}$$

$$\frac{\partial(\rho_\mathrm{p}h_\mathrm{p})}{\partial t} + \boldsymbol{\nabla}\cdot(\rho_\mathrm{p}h_\mathrm{p}\boldsymbol{u}_\mathrm{p}) + \boldsymbol{\nabla}\cdot\Big(-\lambda_\mathrm{p}\boldsymbol{\nabla}T_\mathrm{p} + \int\rho_\mathrm{p}Y^\mathrm{p}(v)\mathfrak{h}(v)\boldsymbol{\mathcal{V}}^\mathrm{p}(v)\,\mathrm{d}v\Big) = \dot{H}_\mathrm{pg}, \tag{A.17}$$

where λ_g is gas-phase thermal conductivity relative to the gas temperature, λ_p is the particle-phase thermal conductivity relative to the particle temperature, $\dot{H}_\mathrm{gp} = -\dot{H}_\mathrm{pg}$ is the enthalpy exchanged between the gas and particle phases, and h_g and h_p denote the gas-phase and particle-phase specific enthalpies, respectively given by:

$$h_\mathrm{g} = \sum_{k=1}^{N_\mathrm{g}} Y_k^\mathrm{g}h_k, \tag{A.18}$$

$$h_\mathrm{p} = \int Y^\mathrm{p}(v)\mathfrak{h}(v)\,\mathrm{d}v. \tag{A.19}$$

The mixture enthalpy is then obtained from:

$$h = Y_\mathrm{g}h_\mathrm{g} + Y_\mathrm{p}h_\mathrm{p}. \tag{A.20}$$

It is worth noting that, in such a dispersed two-phase phase flow, gaseous molecules and solid particles are mixed and interact continuously with each other. Therefore, the thermal flux is the result of the combined effect of collisions between two gaseous molecules, between two solid particles, or between one gaseous molecule and one solid particle. This intricate effect is not linear, i.e. the

thermal conductivities λ_{g}, λ_{p} are not equal to the respective thermal conductivities of the gas phase – computed as if there was no solid particles – and the particle phase – computed as if there was no gaseous molecules, but depend on the composition and characteristics of the other phase. In the case of vanishing nanoparticle mass fraction, then the contribution of the solid particles vanishes and λ_{g} becomes equal to the pure gas phase thermal conductivity, but in general it is not true. The actual expressions for the conductivities λ_{g}, λ_{p} can be derived from kinetic theory [50], and additional couplings might occur between the two phases, but it is beyond the scope of the present article. Finally, if one considers momentum and thermal exchange terms as relaxation terms, then when the relaxation times tend to zero one obtains $\boldsymbol{u}_{\mathrm{g}} = \boldsymbol{u}_{\mathrm{p}}$ and $T_{\mathrm{g}} = T_{\mathrm{p}}$.

B Sectional model

B.1 Particle size distribution discretization

Inside each section i, the particle volume fraction density $q(v) = v\, n(v)$ is considered constant and equal to $q_i = q(v_i^{\mathrm{mean}})$ with $v_i^{\mathrm{mean}} = (v_i^{\mathrm{min}} + v_i^{\mathrm{max}})/2$. The particle number density $n(v)$ for each section i is then evaluated as:

$$n(v) = q_i/v, \quad v \in [v_i^{\mathrm{min}}, v_i^{\mathrm{max}}]. \tag{B.1}$$

Then the particles volume fraction Q_i and the particles number density N_i relative to the section i read:

$$\begin{aligned} Q_i &= \int_i q(v)\, dv = q_i \left(v_i^{\mathrm{max}} - v_i^{\mathrm{min}}\right), \\ N_i &= \int_i n(v)\, dv = q_i \int_i \frac{dv}{v} = q_i \ln\left(\frac{v_i^{\mathrm{max}}}{v_i^{\mathrm{min}}}\right). \end{aligned} \tag{B.2}$$

The total particle volume fraction f_{v} and number density N_{p} are evaluated as:

$$\begin{aligned} f_{\mathrm{v}} &= \int_0^\infty q(v)\, dv = \sum_{i=1}^{N_{\mathrm{s}}} Q_i = \sum_{i=1}^{N_{\mathrm{s}}} q_i \left(v_i^{\mathrm{max}} - v_i^{\mathrm{min}}\right), \\ N_{\mathrm{p}} &= \int_0^\infty n(v)\, dv = \sum_{i=1}^{N_{\mathrm{s}}} N_i = \sum_{i=1}^{N_{\mathrm{s}}} q_i \ln\left(\frac{v_i^{\mathrm{max}}}{v_i^{\mathrm{min}}}\right). \end{aligned} \tag{B.3}$$

We suppose the particles are spherical, so that the surface of a particle of volume v reads:

$$s(v) = \pi^{1/3}(6v)^{2/3}. \tag{B.4}$$

and the diameter reads $d_p = (6v/\pi)^{1/3}$. The particle size distribution discretization is done as follows:

- The first section is defined so that it contains all the nascent particles generated from the nucleation process,
- For $i \in [\![2, N_{\mathrm{sect}} - 1]\!]$, the volume intervals of the sections follow a geometrical progression:

$$\begin{aligned} v_i^{\mathrm{max}} &= v_1^{\mathrm{max}} \left(\frac{v^{\mathrm{MAX}}}{v_1^{\mathrm{max}}}\right)^{\frac{i-1}{N_{\mathrm{sect}}-2}}, \\ v_i^{\mathrm{min}} &= v_{i-1}^{\mathrm{max}}. \end{aligned} \tag{B.5}$$

- The last section can be considered as a "trash" section which contains very big unexpected particles from v^{MAX} to v^{BIG} and guarantees particles mass conservation. The value of v^{BIG} is chosen as an unattainable particle volume. The value of v^{MAX} corresponds to a characteristic volume of the expected biggest particles and is chosen as the maximum particle volume resolved accurately.

The mean molar mass of particles in the i^{th} section is given by

$$W_i = \rho_{\mathrm{s}} \frac{v_i^{\max} - v_i^{\min}}{\ln\left(\frac{v_i^{\max}}{v_i^{\min}}\right)} \mathcal{N}_{\mathrm{A}}. \tag{B.6}$$

B.2 Balance equations of the sectional model

In the particle sectional approach, the particle distribution is discretized in N_{s} sections. Each section i represents particles with a volume between $v_i^{\min}$ and $v_i^{\max}$. The balance equation for the volume fraction Q_i of particles in section i can be derived from the aerosol General Dynamic Equation, and reads:

$$\frac{\partial Q_i}{\partial t} + \boldsymbol{\nabla} \cdot \left(Q_i \left(\mathbf{u} + \boldsymbol{\mathcal{V}}_i\right)\right) = \dot{Q}_i, \tag{B.7}$$

where $\mathbf{u}$ is the gas velocity, $\boldsymbol{\mathcal{V}}_i$ is the diffusion velocity of particles in the i^{th} section, and $\dot{Q}_i$ is the particle volume fraction production rate (in s^{-1}) for the i^{th} section. The particles diffusion coefficients are classically expressed as in the *free molecular* regime [32,51]:

$$D_i = \frac{k_b T}{\left(1 + \frac{\alpha_{\mathrm{T}} \pi}{8}\right) \frac{\pi}{3} n \mathfrak{m} \bar{c} d_i^2}, \tag{B.8}$$

where $\mathfrak{m}$ is the average mass of a gas particle, n is the gas number density, $\bar{c} = \sqrt{\frac{8 k_b T}{\pi \mathfrak{m}}}$ is the brownian velocity of the gas particles where k_b is the Boltzmann constant, d_i is the mean particle diameter in the i^{th} section, α_{T} is the thermal accomodation factor representing the fraction of the gas molecules that leave the surface in equilibrium with the surface, the remaining fraction $1 - \alpha_{\mathrm{T}}$ being specularly reflected: this constant is usually taken equal to $\alpha_{\mathrm{T}} = 0.9$ [32,35].

Noting V_i (respectively M_i) the total volume (respectively the total mass) of particles belonging to section i, and V (respectively M) the total volume (respectively the total mass) of the considered system, the volume fraction Q_i corresponding to the i^{th} section can be expressed as a function of a mass fraction relative to the section i, Y_i, the gas density ρ, and the density of solid particles ρ_{s}:

$$Q_i = \frac{V_i}{V} = \frac{M_i}{\rho_{\mathrm{s}} V} = \frac{Y_i M}{\rho_{\mathrm{s}} V} = \frac{\rho}{\rho_{\mathrm{s}}} Y_i. \tag{B.9}$$

Then, the particles mass fraction Y_i of the section i follows the corresponding transport equation:

$$\frac{\partial (\rho Y_i)}{\partial t} + \boldsymbol{\nabla} \cdot \left(\rho Y_i \left(\mathbf{u} + \boldsymbol{\mathcal{V}}_i\right)\right) = \rho_{\mathrm{s}} \dot{Q}_i, \tag{B.10}$$

where ρ is the mixture density and ρ_{s} is the constant particle density.

The production rate $\dot{Q}_i$ of the particle volume fraction for the i^{th} section incorporates nucleation, coagulation, and surface growth.

C 1D premixed equations for two-phase flow

The 1D premixed model in the Regath code [43,48] is presented here. In the configurations studied here, the low Mach number approximation applies and the momentum equation is not needed. The steady 1D premixed balance equations read classically:

- *Mass conservation:*

$$\frac{d(\rho v)}{dx} = 0. \tag{C.1}$$

- *Species conservation:*

$$\rho v \frac{dY_k}{dx} = -\frac{d}{dx}(\rho Y_k V_k) + W_k \dot{\omega}_k. \tag{C.2}$$

- *Nanoparticle section mass fractions Y_i:*

$$\rho v \frac{dY_i}{dx} = -\frac{d}{dx}\left(\rho Y_i V_i\right) + \rho_s \dot{Q}_i. \tag{C.3}$$

- *Energy conservation:*

$$\rho v \frac{dh}{dx} = -\frac{d}{dx}\left(-\lambda \frac{dT}{dx} + \sum_{k=1}^{N_\mathrm{g}} \rho Y_k h_k V_k + \sum_{i=1}^{N_\mathrm{s}} \rho Y_i h_i V_i\right). \tag{C.4}$$

  It is important to note here that the equation for the axial momentum is decoupled from the other equations, and is only needed for the calculation of the hydrodynamic pressure. Generally, this equation is not solved since it is not necessary in order to obtain the variables of interest.

Boundary conditions

- Boundary conditions at $x = -\infty$:

  The following boundary conditions are applied in the fresh gases:

$$\begin{cases} (\rho v)(-\infty) = (\rho v)^{-\infty} \\ T(-\infty) = T^{-\infty} \\ Y_k(-\infty) = Y_k^{-\infty}, \quad k = 1, \ldots, N_\mathrm{g} \\ Y_i(-\infty) = Y_i^{-\infty}, \quad i = 1, \ldots, N_\mathrm{s} \end{cases} \tag{C.5}$$

  where $T^{-\infty}$, $Y_k^{-\infty}$, $Y_i^{-\infty}$ and $(\rho v)^{-\infty}$, respectively, correspond to the gas temperature, the k^{th} species mass fraction, the i^{th} particle section mass fraction and the mass flow rate, respectively, in the fresh gases at $-\infty$.

- Boundary conditions at $x = +\infty$:

  The following boundary conditions are applied in the burnt gases:

$$\begin{cases} \dfrac{dT}{dx}(+\infty) = 0 \\ \dfrac{dY_k}{dx}(+\infty) = 0, \quad k = 1, \ldots, N_\mathrm{g} \\ \dfrac{dY_i}{dx}(+\infty) = 0, \quad i = 1, \ldots, N_\mathrm{s} \end{cases} \tag{C.6}$$

Note that there is only one boundary condition for the axial velocity, as equation (C.1) is first order.

D 1D counterflow equations

We are working here in a cartesian 2D geometry: x is the direction normal to the flame front, and y is the transverse direction. The origin is chosen so that the stagnation plane is located at $x = 0$. The velocity is decomposed along x and y directions:

$$\boldsymbol{u}(x, y) = v(x, y)\, \boldsymbol{e}_x + u(x, y)\, \boldsymbol{e}_y. \tag{D.1}$$

The strained flow balance equations are obtained when the solution is self-similar, namely [52]:

$$v = v(x), \tag{D.2}$$
$$u = y\, \hat{u}(x), \tag{D.3}$$
$$\rho = \rho(x), \tag{D.4}$$
$$\tilde{p} = -\kappa \frac{y^2}{2} + \hat{p}(x), \tag{D.5}$$
$$T = T(x), \tag{D.6}$$
$$Y_k = Y_k(x), \quad k = 1, \ldots, N_\mathrm{g}, \tag{D.7}$$
$$Y_i = Y_i(x), \quad i = 1, \ldots, N_\mathrm{s}. \tag{D.8}$$

Here, $\tilde{p}$ is the hydrodynamic pressure and κ is the pressure curvature, assumed constant: the strain rate $\alpha = \sqrt{\kappa/\rho^{+\infty}}$ – where $\rho^{+\infty}$ is the density of the fresh gases at $+\infty$ – is imposed. It is then possible to show from the expression of the diffusion velocities that:

$$\boldsymbol{\mathcal{V}}_k = V_k(x)\, \boldsymbol{e}_x, \quad k = 1, \ldots, N_\mathrm{g}, \tag{D.9}$$
$$\boldsymbol{\mathcal{V}}_i = V_i(x)\, \boldsymbol{e}_x, \quad i = 1, \ldots, N_\mathrm{s}. \tag{D.10}$$

The steady strained flow equations then read:

- *Mass conservation:*
$$\frac{d(\rho v)}{dx} + \rho \hat{u} = 0. \tag{D.11}$$

- *Radial momentum equation:*
$$\rho v \frac{d\hat{u}}{dx} + \rho \hat{u}^2 = \kappa + \frac{d}{dx}\left(\mu \frac{d\hat{u}}{dx}\right). \tag{D.12}$$

- *Energy conservation:*
$$\rho v \frac{dh}{dx} = -\frac{d}{dx}\left(-\lambda \frac{dT}{dx} + \sum_{k=1}^{N_\mathrm{g}} \rho Y_k h_k V_k + \sum_{i=1}^{N_\mathrm{s}} \rho Y_i h_i V_i\right). \tag{D.13}$$

- *Species conservation:*
$$\rho v \frac{dY_k}{dx} = -\frac{d}{dx}(\rho Y_k V_k) + W_k \dot{\omega}_k. \tag{D.14}$$

- *Nanoparticle section mass fractions Y_i:*
$$\rho v \frac{dY_i}{dx} = -\frac{d}{dx}\left(\rho Y_i V_i\right) + \rho_s \dot{Q}_i. \tag{D.15}$$

It is important to note here that the equation for the axial momentum is decoupled from the other equations. Generally, this equation is not solved since it is not necessary in order to obtain the variables of interest. Solving this equation allows to obtain the axial pressure gradient.

Boundary conditions

- Boundary conditions at $x = 0$:

$$v = 0 \tag{D.16}$$

- Boundary conditions at $x = -\infty$:

  The following boundary conditions are applied at $-\infty$:

$$\begin{cases} \hat{u}(-\infty) = \alpha\sqrt{\rho^{+\infty}/\rho^{-\infty}} \\ T(-\infty) = T^{-\infty} \\ Y_k(-\infty) = Y_k^{-\infty}, \quad k = 1, \ldots, N_\mathrm{g} \\ Y_i(-\infty) = Y_i^{-\infty}, \quad i = 1, \ldots, N_\mathrm{s} \end{cases} \tag{D.17}$$

  where $\rho^{-\infty}$, $T^{-\infty}$, $Y_k^{-\infty}$ and $Y_i^{-\infty}$, respectively, correspond to the density, the gas temperature, the k^{th} species mass fraction, the i^{th} particle section mass fraction, respectively, in the fresh gases at $x = -\infty$, and $\rho^{+\infty}$ is the density in the fresh gases at $x = +\infty$.

- Boundary conditions at $x = +\infty$:

  The following boundary conditions are applied at $+\infty$:

$$\begin{cases} \hat{u}(+\infty) = \alpha \\ T(+\infty) = T^{+\infty} \\ Y_k(+\infty) = Y_k^{+\infty}, \quad k = 1, \ldots, N_\mathrm{g} \\ Y_i(+\infty) = Y_i^{+\infty}, \quad i = 1, \ldots, N_\mathrm{s} \end{cases} \tag{D.18}$$

  where $T^{+\infty}$, $Y_k^{+\infty}$ and $Y_i^{+\infty}$, respectively, correspond to the gas temperature, the k^{th} species mass fraction, the i^{th} particle section mass fraction, respectively, in the fresh gases at $x = +\infty$.

References

[1] Pratsinis E 1998 *Prog. Energy Combust. Sci.* **23** 197–219 1

[2] Kelesidis G A, Goudeli E and Pratsinis S E 2017 *Proceedings of the Combustion Institute* **36** 29–50 ISSN 15407489 URL https://linkinghub.elsevier.com/retrieve/pii/S1540748916304679 1

[3] Marchisio D L and Fox R O 2013 *Computational Models for Polydisperse Particulate and Multiphase Systems* (Cambridge University Press) 1

[4] Raman V and Fox R O 2016 *Annual Review of Fluid Mechanics* **48** 159–190 ISSN 0066-4189, 1545-4479 URL http://www.annualreviews.org/doi/10.1146/annurev-fluid-122414-034306 1

[5] George P 1973 *Faraday Symposia of the Chemical Society* **7** 63–71 2

[6] Pratsinis S E, Zhu W and Vemury S 1996 *Powder Technology* **86** 87–93 ISSN 00325910 URL http://linkinghub.elsevier.com/retrieve/pii/0032591095030417 2

[7] Zhu W and Pratsinis S E 1996 Flame Synthesis of Nanosize Powders: Effect of Flame Configuration and Oxidant Composition *Nanotechnology* (*ACS Symposium Series* vol 622) ed Chow G M and Gonsalves K E (Washington, DC: American Chemical Society) pp 64–78 URL http://pubs.acs.org/doi/abs/10.1021/bk-1996-0622.ch004 2

[8] Pratsinis S E, Bai H, Biswas P, Frenklach M and Mastrangelo S V R 1990 *Journal of the American Ceramic Society* **73** 2158–2162 ISSN 0002-7820, 1551-2916 URL http://doi.wiley.com/10.1111/j.1151-2916.1990.tb05295.x 2, 9

[9] Heine M C and Pratsinis S E 2007 *Particle & Particle Systems Characterization* **24** 56–65 ISSN 09340866 URL http://doi.wiley.com/10.1002/ppsc.200601076 2, 3, 9

[10] Hwang J Y, Gil Y S, Kim J I, Choi M and Chung S H 2001 *Aerosol Science* 13 2

[11] Kim H J, Jeong J I, Park Y, Yoon Y and Choi M 2003 *Journal of Nanoparticle Research* **5** 237–246 2

[12] Lee B, Oh S and Choi M 2001 *Aerosol Science and Technology* **35** 978–989 ISSN 0278-6826, 1521-7388 URL http://www.tandfonline.com/doi/abs/10.1080/02786820175330674 1 2

[13] GrÃűhn A J, Buesser B, Jokiniemi J K and Pratsinis S E 2011 *Industrial & Engineering Chemistry Research* **50** 3159–3168 ISSN 0888-5885, 1520-5045 URL http://pubs.acs.org/doi/abs/10.1021/ie1017817 2

[14] Pratsinis S E and Spicer P T 1998 *Chemical Engineering Science* **53** 1861–1868 ISSN 00092509 URL http://linkinghub.elsevier.com/retrieve/pii/S0009250998000268 2, 9, 11

[15] Spicer P T, Chaoul O, Tsantilis S and Pratsinis S E 2002 *Journal of Aerosol Science* **33** 17–34 ISSN 00218502 URL http://linkinghub.elsevier.com/retrieve/pii/S0021850201000696 2, 9, 11

[16] Tsantilis S and Pratsinis S E 2004 *Journal of Aerosol Science* **35** 405–420 ISSN 00218502 URL http://linkinghub.elsevier.com/retrieve/pii/S0021850203004415 2, 9, 11

[17] Morgan N, Wells C, Goodson M, Kraft M and Wagner W 2006 *Journal of Computational Physics* **211** 638–658 ISSN 00219991 URL http://linkinghub.elsevier.com/retrieve/pii/S0021999105002913 2, 9, 11

[18] Boje A, Akroyd J, Sutcliffe S, Edwards J and Kraft M 2017 *Chemical Engineering Science* **164** 219–231 ISSN 00092509 URL https://linkinghub.elsevier.com/retrieve/pii/S0009250917301276 2

[19] West R H, Shirley R A, Kraft M, Goldsmith C F and Green W H 2009 *Combustion and Flame* **156** 1764–1770 ISSN 00102180 URL http://linkinghub.elsevier.com/retrieve/pii/S0010218009001163 2

[20] Mehta M, Sung Y, Raman V and Fox R O 2010 *Industrial & Engineering Chemistry Research* **49** 10663–10673 ISSN 0888-5885, 1520-5045 URL http://pubs.acs.org/doi/abs/10.1021/ie100560h 2, 9

[21] Mehta M, Raman V and Fox R O 2013 *Chemical Engineering Science* **104** 1003–1018 ISSN 00092509 URL http://linkinghub.elsevier.com/retrieve/pii/S0009250913007264 2

[22] Johannessen T, Pratsinis S E and Livbjerg H 2001 *Powder Technology* **118** 242–250 ISSN 00325910 URL http://linkinghub.elsevier.com/retrieve/pii/S0032591000004010 2

[23] Sung Y, Raman V and Fox R O 2011 *Chemical Engineering Science* **66** 4370–4381 ISSN 00092509 URL http://linkinghub.elsevier.com/retrieve/pii/S0009250911002661 2

[24] Sung Y, Raman V, Koo H, Mehta M and Fox R O 2014 *AIChE Journal* **60** 459–472 ISSN 00011541 URL http://doi.wiley.com/10.1002/aic.14279 2

[25] Akroyd J, Smith A J, Shirley R, McGlashan L R and Kraft M 2011 *Chemical Engineering Science* **66** 3792–3805 ISSN 00092509 URL http://linkinghub.elsevier.com/retrieve/pii/S0009250911003009 2, 6

[26] Wang G and Garrick S C 2005 *Journal of Nanoparticle Research* **7** 621–632 ISSN 1388-0764, 1572-896X URL http://link.springer.com/10.1007/s11051-005-4966-7 2, 9

[27] Garrick S C and Wang G 2011 *Journal of Nanoparticle Research* **13** 973–984 ISSN 1388-0764, 1572-896X URL http://link.springer.com/10.1007/s11051-010-0097-x 2

[28] Xu Z, Zhao H and Zhao H 2017 *Proceedings of the Combustion Institute* **36** 1099–1108 ISSN 15407489 URL https://linkinghub.elsevier.com/retrieve/pii/S1540748916302644 2

[29] Park S H, Kruis F E, Lee K W and Fissan H 2002 *Aerosol Science and Technology* **36** 419–432 ISSN 0278-6826, 1521-7388 URL https://www.tandfonline.com/doi/full/10.1080/027868202753571241 3

[30] Kruis F E and Kusters K A 1997 *Chemical Engineering Communications* **158** 201–230 ISSN 0098-6445, 1563-5201 URL https://www.tandfonline.com/doi/full/10.1080/00986449708936589 3

[31] Buesser B, Heine M and Pratsinis S 2009 *Journal of Aerosol Science* **40** 89–100 ISSN 00218502 URL http://linkinghub.elsevier.com/retrieve/pii/S0021850208001730 3

[32] Friedlander S and Friedlander P 2000 *Smoke, Dust, and Haze: Fundamentals of Aerosol Dynamics* Topics in chemical engineering (Oxford University Press) ISBN 978-0-19-512999-1 URL https://books.google.fr/books?id=fNIeNvd3Ch0C 3, 20

[33] Giovangigli V 1990 *Impact of Computing in Science and Engineering* **2** 73–97 5, 7

[34] Derjaguin B V, Storozhilova A I and Rabinovich Y I 1966 *Journal of Colloid and Interface Science* **21** 35–58 5

[35] Waldmann L and Schmitt K 1966 Thermophoresis and diffusiophoresis of aerosols *Aerosol Science* (Academic Press, New York) pp 137–162 davies, c. n. ed 5, 20

[36] Boyd R and Kent J 1988 *Symposium (International) on Combustion* **21** 265–274 ISSN 00820784 URL https://linkinghub.elsevier.com/retrieve/pii/S0082078488802546 6

[37] Xiong Y, Kamal Akhtar M and Pratsinis S E 1993 *Journal of Aerosol Science* **24** 301–313 ISSN 00218502 URL http://linkinghub.elsevier.com/retrieve/pii/002185029390004S 9

[38] Smith G P, Golden D M, Frenklach M, Moriarty N W, Eiteneer B, Goldenberg M, Bowman C T, Hanson R K, Song S, Gardiner Jr W C, Lissianski V V and Qin Z GRI-Mech 3.0 URL http://www.me.berkeley.edu/gri_mech/ 9

[39] Mehta M, Fox R O and Pepiot P 2015 *Industrial & Engineering Chemistry Research* **54** 5407–5415 ISSN 0888-5885, 1520-5045 URL http://pubs.acs.org/doi/10.1021/acs.iecr.5b00130 9

[40] Gelbard F, Tambour Y and Seinfeld J H 1980 *Journal of Colloid and Interface Science* **76** 541–556 ISSN 00219797 URL https://linkinghub.elsevier.com/retrieve/pii/002197978090394X 10

[41] Chapman S and Cowling T G 1970 *The Mathematical Theory of Non-uniform Gases: An Account of the Kinetic Theory of Viscosity, Thermal Conduction and Diffusion in Gases* (Cambridge University Press) 10

[42] Marchal C 2008 *ModÃľlisation de la formation et de l'oxydation des suies dans un moteur automobile* Ph.D. thesis UniversitÃľ d'OrlÃľans 10

[43] Rodrigues P 2018 *ModÃľlisation multiphysique de flammes turbulentes suitÃľes avec la prise en compte des transferts radiatifs et des transferts de chaleur pariÃľtaux.* Ph.D. thesis UniversitÃľ Paris-Saclay 10, 11, 13, 20

[44] Sutherland W 1893 *The London, Edinburgh, and Dublin Philosophical Magazine and Journal of Science* **36** 507–531 ISSN 1941-5982, 1941-5990 URL https://www.tandfonline.com/doi/full/10.1080/14786449308620508 10

[45] Cunningham E 1910 *Proceedings of the Royal Society A: Mathematical, Physical and Engineering Sciences* **83** 357–365 ISSN 1364-5021, 1471-2946 URL http://rspa.royalsocietypublishing.org/cgi/doi/10.1098/rspa.1910.0024 10

[46] Pratsinis S E 1988 *Journal of Colloid and Interface Science* **124** 416–427 ISSN 00219797 URL http://linkinghub.elsevier.com/retrieve/pii/0021979788901804 10

[47] Ghoshtagore R N 1970 *Journal of The Electrochemical Society* **117** 529 ISSN 00134651 URL http://jes.ecsdl.org/cgi/doi/10.1149/1.2407561 11

[48] Rodrigues P, Franzelli B, Vicquelin R, Gicquel O and Darabiha N 2017 *Proceedings of the Combustion Institute* **36** 927–934 ISSN 15407489 URL https://linkinghub.elsevier.com/retrieve/pii/S1540748916303054 11, 13, 20

[49] West R H, Beran G J O, Green W H and Kraft M 2007 *The Journal of Physical Chemistry A* **111** 3560–3565 ISSN 1089-5639, 1520-5215 URL http://pubs.acs.org/doi/abs/10.1021/jp0661950 12

[50] OrlacâĂŹh J M, Giovangigli V, Novikova T and RocaÂăiÂăCabarrocas P 2018 *Physica A: Statistical Mechanics and its Applications* **494** 503–546 ISSN 03784371 URL https://linkinghub.elsevier.com/retrieve/pii/S0378437117312323 19

[51] Epstein P S 1924 *Physical Review* **23** 710–733 ISSN 0031-899X URL https://link.aps.org/doi/10.1103/PhysRev.23.710 20

[52] Giovangigli V 1999 *Multicomponent Flow Modeling* (BirkhÃď user) 22